ANNUAL REVIEWS

Annual Review of Nuclear and Particle Science

Short-Lived Nuclides in the Early Solar System: Abundances, Origins, and Applications

Andrew M. Davis

Department of the Geophysical Sciences, Enrico Fermi Institute, and Chicago Center for Cosmochemistry, The University of Chicago, Chicago, Illinois, USA;
email: a-davis@uchicago.edu

Annu. Rev. Nucl. Part. Sci. 2022. 72:339–63

First published as a Review in Advance on July 14, 2022

The *Annual Review of Nuclear and Particle Science* is online at nucl.annualreviews.org

https://doi.org/10.1146/annurev-nucl-010722-074615

Keywords

short-lived radionuclides, chronology, nucleosynthesis, meteorites, early Solar System, planet formation

Abstract

Several short-lived radionuclides (SLRs) were present in the first few million years of Solar System history. Their abundances have profound impact on the timing of stellar nucleosynthesis events prior to Solar System formation, chronology of events in the early Solar System, early solar activity, heating of early-formed planetesimals, and chronology of planet formation. Isotopic analytical techniques have undergone dramatic improvements in the past decade, leading to tighter constraints on the levels of SLRs in the early Solar System and on the use of these nuclides for detailed chronological studies. This review emphasizes the abundances of SLRs when the Solar System formed and how we know them, and briefly discusses the origins of these nuclides and applications in planetary science.

Contents

INTRODUCTION

Many short-lived radionuclides (SLRs) were present in the first few million years of Solar System history. Their presence is inferred through excesses in daughter isotopes (compared to normal terrestrial isotopic composition) in various materials found in primitive meteorites. Studies of SLRs have been underway for more than 60 years, beginning with the discovery of excess ^{129}Xe from ^{129}I ($T_{1/2}$ = 16.14 Ma) (1), but even before that, ^{26}Al ($T_{1/2}$ = 0.717 Ma) was appealed to as a source of heat for melting asteroids (2). There are now 14 confirmed SLRs that were present at the birth of the Solar System, the most recent being ^{247}Cm (3, 4), along with 4 SLRs with significant upper limits. Several comprehensive reviews of the SLRs and their application to early Solar System (ESS) chronology have been written, with the most recent ones written about a decade ago (5, 6). Rather than repeat what has been written in those reviews, I have chosen to

emphasize progress made in the decade since the last one (6) was written in 2012, starting with a description of how ESS SLR abundances are determined, continuing with current estimates of SLR abundances, and concluding with brief discussions of sources of SLRs and impacts on planetary science.

MEASUREMENTS AND A LITTLE COSMOCHEMISTRY

Measurements

Detailed studies of the abundances of SLRs require high-precision isotope ratio measurements on samples or subsamples with relatively low parent-to-daughter ratios or high spatial resolution measurements on individual phases that have high parent-to-daughter ratios. The field of SLRs in the ESS has blossomed in the past couple of decades with refinement of two important analytical techniques, multicollector inductively coupled plasma mass spectrometry (MC-ICPMS) and multicollector secondary ion mass spectrometry (MC-SIMS), particularly for significantly improved precision of measurements of small excesses in the abundances of daughter isotopes. Also important has been the development of laser resonance ionization mass spectrometry (RIMS) and intense, well-focused primary ion beams for SIMS.

Bulk Measurements

Measurements of bulk meteorites and inclusions within them are now predominantly done by MC-ICPMS (7), although important contributions by thermal ionization mass spectrometry (TIMS) have also been made (8). For both ICPMS and TIMS, careful dissolution and chemical separation of the element of interest, usually in a sophisticated clean laboratory, are necessary.

In ICPMS, an aerosol is generated from an aqueous solution of the sample and introduced into an argon plasma torch at 1 atm, where essentially all elements are efficiently ionized, predominantly to a charge of +1. This plasma torch is aimed at a small hole in a cone, which introduces the plasma into the vacuum system of the mass spectrometer, where the ions are accelerated, focused, mass analyzed, and detected. In the MC-ICPMS instruments used for high-precision isotopic work, an array of ion detectors is used to simultaneously collect all isotopes of the element of interest. These detectors can be Faraday cups for intense beams or electron multipliers for lower-intensity beams. The ICPMS has the advantage that nearly any element can be isotopically analyzed with high efficiency; however, the ions are made in a 1-atm plasma and must be introduced into the vacuum system of the mass spectrometer. This comes at a considerable cost in useful yield (ions counted in detectors per atom introduced into the plasma). The high ionization efficiency can also be a disadvantage, as it requires clean separation of the element of interest from other elements having isobars (e.g., ^{58}Fe and ^{58}Ni). There can be subtle effects on isotopic composition from other noninterfering elements in solution or from acid strength, so it is important to match the chemical composition of sample and standard solutions. Compared with TIMS, ICPMS has the advantage that one can rapidly switch between introducing sample or standard into the plasma, and sample-standard bracketing is the normal mode of operation. This capability allows precise measurement of natural mass-dependent isotopic fractionation effects. For example, current analytical techniques used for magnesium by MC-ICPMS give isotope ratio precisions of a few parts per million (9).

In TIMS, a solution of the element of interest is evaporated onto a filament made of a refractory element, such as tantalum. The filament is then placed inside the mass spectrometer vacuum system and heated until singly charged positive (or negative) ions are generated. These ions are then accelerated, energy filtered, mass analyzed, and detected with a multiple collector array. It is not practical to frequently switch between filaments loaded with sample and standard;

furthermore, varying degrees of isotopic mass fractionation occur during thermal evaporation, so TIMS is significantly less precise than MC-ICPMS for mass-dependent isotopic fractionation measurements. There is a significant range in ionization efficiency for different elements and the community can be secretive about chemical separation techniques and elements or compounds to add to the filament to increase ionization efficiency. For mass-independent fractionation effects, due to radioactive decay of a parent isotope or due to isotopic variations of nucleosynthetic origin, both MC-TIMS and MC-ICPMS can achieve precisions of a few parts per million.

In Situ Measurements

Nearly all in situ isotopic data used to infer the former presence of SLRs come from SIMS using either a multicollector for intense secondary ion beams or a single collector for some low-concentration measurements (10). Laser ablation MC-ICPMS, in which aerosol particles generated by laser ablation of samples are introduced into the plasma torch, has seen limited use in the study of SLRs. This technique has the advantage of speed and avoidance of chemical separation, but all elements in the sample are ionized, often leading to isobaric interferences.

The limited useful yield (atoms detected per atom removed from the sample) of SIMS and ICPMS and isobaric interferences in SIMS and laser ablation ICPMS have motivated the development of RIMS, in which sputtered or laser-ablated neutral atoms are resonantly ionized by several tunable lasers. This technique offers the ability to ionize only the element of interest, practically eliminating isobaric interferences, as well as a high useful yield (11, 12).

Complicating Factors

Studying SLRs via mass spectrometry can incur complications. Isobaric interferences can cause issues in SIMS or laser ablation ICPMS measurements, in which ions of many elements can be introduced into mass spectrometers, and in ICPMS or TIMS when chemical separations are incomplete. Some of these interferences can be eliminated by operating at high mass resolution. For example, in SIMS, $^{48}Ca^{2+}$ interference on $^{24}Mg^{+}$, or $^{24}MgH^{+}$ interference on $^{25}Mg^{+}$, can be eliminated by operating at a mass resolution ($M/\Delta M$) of a few thousand, which modern instruments are capable of. Other interferences, such as $^{58}Fe^{+}$ on $^{58}Ni^{+}$, which is useful for studying the ^{60}Fe-^{60}Ni system, require mass resolution beyond the capability of even large-radius instruments such as the Cameca IMS-1280 SIMS or Nu Plasma 1700 ICPMS, but can be dealt with by ICPMS or TIMS with chemical separations or by RIMS (11).

Some SLR systems have been studied only by high-precision isotopic analyses on samples with low parent/daughter ratios, such as the ^{182}Hf-^{182}W system. Here, exposure to cosmic rays for tens to hundreds of millions of years can modify isotope ratios due largely to neutron-capture effects from secondary neutrons generated by galactic cosmic rays. For tungsten isotopic studies of iron meteorites, platinum isotopes have been used to correct for cosmic-ray exposure effects.

Finally, isotopic mass fractionation, which is a function of mass differences between pairs of isotopes, can occur in nature, due to kinetic and equilibrium effects, and in mass spectrometers, due to mass-dependent differences in evaporation of isotopes from filaments in TIMS, in matrix-dependent sputtering of secondary ions in SIMS, or in transport of ions within mass spectrometers. The laws defining the relationship between isotope ratio pairs of elements with three or more isotopes are not the same for different natural or analytical processes. The consequences of this have been explored for magnesium isotopes (13).

A Primer on Meteorites and Their Inclusions

Meteorites can be divided into two major groups: chondrites, which are generally sedimentary rocks that accreted on asteroidal parent bodies, and achondrites, which result from melting and

differentiation of asteroidal parent bodies. Most chondrites have experienced some heating and thermal metamorphism or low-temperature aqueous alteration on their parent bodies, so studies of SLRs have focused on objects from primitive carbonaceous and unequilibrated ordinary chondrites where such effects are minimal. SLRs have also been studied in differentiated meteorites, which include silicate rocks that likely come from Vesta and other differentiated asteroids; stony-iron meteorites from mantles or core-mantle boundaries; and iron meteorites from cores of differentiated asteroids. For more on classification of meteorites, see Reference 14.

The oldest objects formed in the Solar System are calcium-, aluminum-rich inclusions (CAIs). The current widely accepted absolute age of the Solar System comes from the uranium-corrected Pb-Pb dating of leachates from four CAIs, which gives an age of 4567.30 ± 0.16 Ma (15, 16). There is also a slightly older uranium-corrected Pb-Pb age of 4567.94 ± 0.31 Ma, based on mineral separates and leachates of a CAI, published only in an abstract (17) but widely quoted. These CAIs have the highest levels of many SLRs among Solar System materials. CAIs come in many varieties (18). Researchers have conducted many studies of CAIs in CV chondrites (14), which tend to be larger than CAIs in other types of carbonaceous chondrites, commonly up to 1 cm across (18). These CAIs have been subdivided on the basis of mineralogy and bulk chemical composition. Type A CAIs are dominantly melilite ($Ca_2Mg_xAl_{2-2x}Si_{1+x}O_7$) and spinel ($MgAl_2O_4$), with minor amounts of perovskite ($CaTiO_3$), hibonite ($CaMg_xTi^{+4}{}_xAl_{12-2x}O_{19}$; $x < 1$), and a Ca-, Al-rich pyroxene widely referred to as fassaite, which is a solid solution of diopside ($CaMgSi_2O_6$), kushiroite ($CaAl_2SiO_6$), grossmanite ($CaTi^{+3}AlSiO_6$), and $CaTi^{+4}Al_2O_6$. Type A CAIs are further subdivided into compact, which appear to have been melted, and fluffy, which may be direct nebular condensates. The Type B CAIs consist of melilite, fassaite, spinel, and anorthite ($CaAl_2Si_2O_8$); these are subdivided into B1 CAIs, which have a melilite-rich mantle, and B2 CAIs, which do not have a mantle. There are also forsterite-rich Type B CAIs (FoBs), which are made of forsterite (Mg_2SiO_4), melilite, fassaite, and spinel. Type C CAIs consist of anorthite, melilite, fassaite, and spinel. All three kinds of Type B CAIs, as well as Type C CAIs, were melted and have fully crystallized, as they contain no glass. Also important are fine-grained CAIs, so named because they are opaque when viewed in a 30-μm-thick polished thin section with an optical microscope. The fine-grained CAIs preserve evidence of high-temperature condensation and evaporation (18, 19), but they have not been melted. CAIs in other kinds of carbonaceous chondrites are smaller, mostly less than approximately 200 μm across, and are Type A, spinel-rich (with spinel, diopside, and perovskite), spinel-hibonite (SHIBs), or monomineralic hibonite crystals [known as platy crystals (PLACs)]. The PLACs and rare Type A or B CAIs in CV chondrites, called FUN (fractionation and unidentified nuclear), have outsized importance relative to their abundance because they have nucleosynthetic isotope anomalies in many elements, and often have large mass-dependent enrichments in heavy isotopes of oxygen, magnesium, and silicon, indicating high-temperature evaporation (20).

Also important are chondrules, spherical silicate balls that were rapidly heated and cooled in space and are the dominant component of chondritic meteorites. They usually consist of olivine ($Mg_{2-x}Fe_xSiO_4$), pyroxene ($Mg_{2-x}Fe_xSi_2O_6$), and calcium-, aluminum-silicate glass. Occasional aluminum-rich chondrules can contain anorthite, which has a high Al/Mg ratio and is important for ^{26}Al-^{26}Mg dating. Amoeboid olivine aggregates are another type of object in carbonaceous chondrites that have some importance for ^{26}Al-^{26}Mg dating. These appear to be predominantly solar nebular condensate aggregates made of forsterite, but they can have inclusions of CAIs. For more on chondrites and their components, see Reference 21.

Another important feature of meteorites that has become recognized in the past decade is that there appear to be two major isotopic reservoirs in the ESS: the CC (carbonaceous chondrites) group, which consists of all types of carbonaceous chondrites and some groups of

iron meteorites, and the NC (noncarbonaceous chondrites) group, which consists of ordinary chondrites, most achondrites (stony, iron, and stony-iron), and the Earth, the Moon, and Mars. It has been suggested that these two groups might have been separated by Jupiter's orbit. The two groups can be recognized by differences in oxygen, calcium, titanium, chromium, iron, nickel, zirconium, molybdenum, ruthenium, and neodymium isotopes (22–24).

Isochron Diagrams

The former presence of an SLR is inferred from an isochron diagram (for an example, see **Figure 1**) in which the isotope ratio of the daughter isotope normalized to a nonradiogenic isotope of the same element is plotted against the ratio of a stable isotope of the element of the short-lived isotope normalized to the same nonradiogenic daughter isotope. If the system is well-behaved, a statistical fit to the data will yield a linear array termed an isochron. The slope of the isochron gives the ratio of the SLR to a nonradioactive isotope of the same element at the time of formation of the object. The intercept of the isochron gives the initial isotope ratio of the daughter isotope normalized to a nonradiogenic isotope of the daughter element. The statistical fit to the isochron should take into account the uncertainties in both the *x*- and *y*-directions for each data point, as well as any correlation between the uncertainties. A commonly used measure of goodness-of-fit is the mean square weighted distribution (MSWD). An MSWD value outside the range $1 \pm 2\sigma_{MSWD}$, where $2\sigma_{MSWD} = \sqrt{2/(n-2)}$ and n is the number of data points, indicates that there is scatter about the isochron beyond that expected from the analytical uncertainties of the data points. Low MSWD values outside this range indicate that uncertainties have been

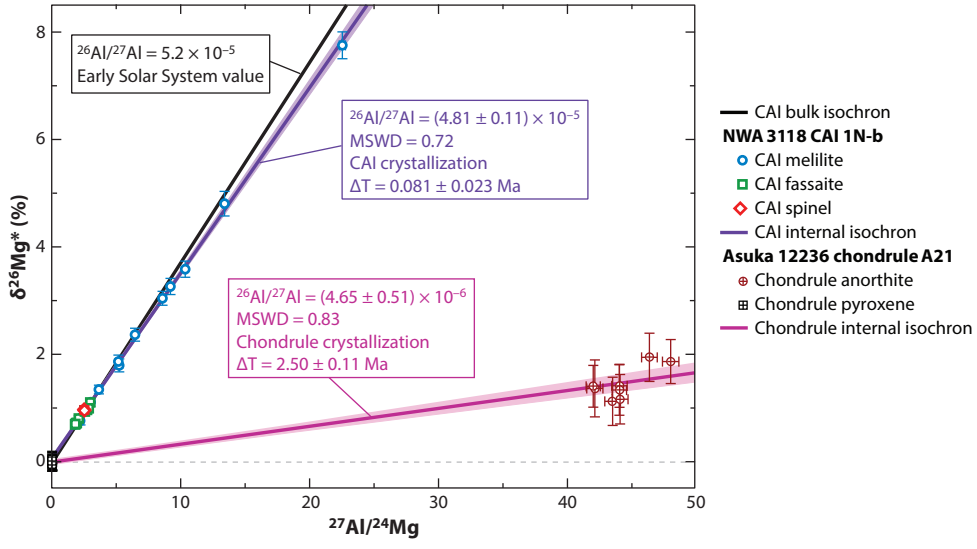

Figure 1

Examples of internal isochrons for the ^{26}Al-^{26}Mg system for CAI 1N-b from the CV chondrite NWA 3118 (150) and for chondrule A21 from the CM2.9 chondrite Asuka 12236 (141). The slopes of the isochrons correspond to the ^{26}Al/^{27}Al atom ratios at the time of crystallization of the two objects. The intercepts of the isochrons give the δ^{26}Mg* values in parts per thousand (‰) of all minerals in each object at the time of crystallization. The δ^{26}Mg* then grows in proportion to the ^{27}Al/^{24}Mg atom ratio as ^{26}Al decays ($T_{1/2} = 0.717$ Ma), reaching the current measured values within a few million years. The crystallization times of the CAI and chondrule are given relative to the initial ^{26}Al/^{27}Al ratio of the Solar System, which comes from bulk CAIs (44, 45) and was established when refractory aluminum was fractionated from less-refractory magnesium by high-temperature processes in the solar nebula. Abbreviation: CAI, calcium-, aluminum-rich inclusion.

overestimated; high MSWD values can have many causes, including partial isotopic exchange of some data points with surrounding phases at a later time, underestimation of uncertainties, and unrecognized interferences. There are also two types of isochrons: internal and bulk. An internal isochron is made from data points collected on individual minerals from a single object formed by crystallization from a melt or solution or by condensation from a vapor. It gives the parent-to-daughter ratio of an SLR at the time of crystallization. A bulk isochron consists of several bulk meteorites or whole CAIs or chondrules; it gives the parent-to-daughter ratio of an SLR at the time of igneous differentiation of an asteroid or at the time of vapor-solid fractionation of elements in the solar nebula leading to an ensemble of objects like CAIs or chondrules. The systematics of isochron diagrams are explained in more detail elsewhere (e.g., 25), but examples of a bulk CAI, an individual CAI, and an individual chondrule ^{26}Al-^{26}Mg isochron are shown in **Figure 1**. Mass spectrometers can measure relative isotope ratios much more precisely than absolute isotope ratios. For this reason, it is common to express isotope ratios as deviations in parts per thousand (δ-values), parts per ten thousand (ε-units), or parts per million (μ-values) relative to a standard material. For example, for magnesium, $\delta^{26}\text{Mg} = [(^{26}\text{Mg}/^{24}\text{Mg})_{\text{sample}}/(^{26}\text{Mg}/^{24}\text{Mg})_{\text{standard}} - 1] \times 1000$. Standard materials are chosen to be uniform in isotopic composition, easily available, and as close as possible to bulk Earth isotopic composition. If isotope ratios have been corrected for mass fractionation effects, they are often designated with an asterisk, e.g., $\delta^{26}\text{Mg}^*$.

EARLY SOLAR SYSTEM ABUNDANCES

ESS SLR abundances are given in order of atomic mass in this section and are current as of 2022. The values are summarized in **Table 1** and discussed in detail below.

^{7}Be

^{7}Be is the shortest-lived radionuclide whose presence has been claimed in Solar System materials; it decays by electron capture to ^{7}Li with a half-life of 53.22 ± 0.06 days (26). This half-life is so short that any ^{7}Be in Solar System materials must be of local origin and cannot be a product of stellar nucleosynthesis. The first reported possible presence of ^{7}Be was in the Type B1 CAI Allende 3529-41 (27). This CAI had a well-defined internal isochron, indicating in situ ^{10}Be decay (see below) but some signs of disturbance of its ^{26}Al-^{26}Mg isochron (28). In the ^{7}Li/^{6}Li versus ^{9}Be/^{6}Li internal isochron, a significant fraction of the data that missed the trajectory expected for closed-system crystal fractionation on a Be versus Li concentration plot was excluded (27). A recalculation of the corrections for cosmogenic lithium isotopes in the sample, based on a new evaluation of cosmic-ray production rates (29), did not change the slope of the isochron, which remained consistent with the original value of $^{7}\text{Be}/^{9}\text{Be} = 0.0061 \pm 0.0013$ (27). However, the correlation does not seem to be linear (29). This is perhaps to be expected because the half-life of ^{7}Be is comparable to the inferred crystallization times of molten CAIs (hours to days). A recently reported isochron from Efremovka 40, a Type B CAI, had a slope corresponding to $^{7}\text{Be}/^{9}\text{Be} = 0.0012 \pm 0.0010$ (30), lower than the original value of 0.0061 ± 0.0013 (27). There is too much scatter in the data to infer the linearity of this correlation. Also, this CAI has an $^{26}\text{Al}/^{27}\text{Al}$ age of 0.45 ± 0.30 Ma after initial formation of CAIs. The possible presence of ^{7}Be in CAIs remains controversial because of the extremely short half-life and the large corrections to lithium isotopic data for cosmic-ray exposure effects. Adding to these complications, lithium is a light element that isotopically fractionates significantly during diffusion and diffuses extremely rapidly (31). Diffusive fractionation of $^{7}\text{Li}/^{6}\text{Li}$ of a few tens of permil, comparable in magnitude to the $^{7}\text{Li}/^{6}\text{Li}$ excesses attributed to ^{7}Be decay, has been found in natural materials, such as Martian basalts (e.g., 32) and chondrules (33). Finally, at low concentrations, analytical uncertainties are

Table 1 SLRs once existing in Solar System objects; shaded rows indicate SLRs with unconfirmed or uncertain abundances

Fractionation[a]	Parent nuclide	Half-life (Ma)[b]	Daughter nuclide	Estimated initial Solar System abundance	Objects found in	Reference(s)
Nebular	^{7}Be	53.22 ± 0.06 d	^{7}Li	$(6.1 \pm 1.3) \times 10^{-3} \times {}^{9}$Be	CAI	27
Nebular	^{10}Be	1.387 ± 0.0012	^{10}B	$(7.3 \pm 1.7) \times 10^{-4} \times {}^{9}$Be	CAIs	36; this article
Nebular, planetary	^{26}Al	0.717 ± 0.024	^{26}Mg	$(5.20 \pm 0.13) \times 10^{-5} \times {}^{27}$Al	CAIs, chondrules, achondrites	44, 45
Planetary	^{36}Cl	0.3013 ± 0.0015	^{36}S, ^{36}Ar	$(1.7–3.0) \times 10^{-5} \times {}^{35}$Cl	CAIs, chondrites	55
Nebular	^{41}Ca	0.0994 ± 0.0015	^{41}K	$4 \times 10^{-9} \times {}^{40}$Ca	CAIs	62
Nebular, planetary	^{53}Mn	3.7 ± 0.4	^{53}Cr	$(7 \pm 1) \times 10^{-6} \times {}^{55}$Mn	CAIs, chondrules, carbonates, achondrites	69
Nebular, planetary	^{60}Fe	2.62 ± 0.04	^{60}Ni	$(1.01 \pm 0.27) \times 10^{-8} \times {}^{56}$Fe	Achondrites, chondrites	79
Planetary	^{92}Nb	34.7 ± 2.4	^{92}Zr	$(1.66 \pm 0.10) \times 10^{-5} \times {}^{93}$Nb	Chondrites, mesosiderites	89
Planetary	^{97}Tc	4.21 ± 0.16	^{97}Mo	$<1 \times 10^{-6} \times {}^{92}$Mo	Iron meteorites	90
Planetary	^{98}Tc	4.2 ± 0.3	^{98}Ru	$<2 \times 10^{-5} \times {}^{96}$Ru	Iron meteorites	91
Planetary	^{107}Pd	6.5 ± 0.3	^{107}Ag	$(5.9 \pm 2.2) \times 10^{-5} \times {}^{108}$Pd	Iron meteorites, pallasites	94
Planetary	^{126}Sn	0.230 ± 0.014	^{126}Te	$<3 \times 10^{-6} \times {}^{124}$Sn	Chondrules, secondary minerals	101
Planetary	^{129}I	16.14 ± 0.12	^{129}Xe	$(1.35 \pm 0.02) \times 10^{-4} \times {}^{127}$I	Chondrules, secondary minerals	This article
Nebular	^{135}Cs	1.33 ± 0.19	^{135}Ba	$<2.8 \times 10^{-6} \times {}^{133}$Cs	CAIs, chondrites	109
Planetary	^{146}Sm	103 ± 5[c]	^{142}Nd	$(8.40 \pm 0.32) \times 10^{-3} \times {}^{144}$Sm	Planetary differentiates	114
Planetary	^{182}Hf	8.90 ± 0.09	^{182}W	$(1.018 \pm 0.043) \times 10^{-4} \times {}^{180}$Hf	CAIs, planetary differentiates	117
Planetary	^{205}Pb	17.0 ± 0.9	^{205}Tl	$(1.8 \pm 1.2) \times 10^{-3} \times {}^{204}$Pb	Chondrites	121
Planetary	^{244}Pu	81.3 ± 0.3	^{232}Th; fission	$(7.7 \pm 0.6) \times 10^{-3} \times {}^{238}$U	CAIs, chondrites	123
Nebular	^{247}Cm	15.6 ± 0.5	^{235}U	$(5.6 \pm 0.3) \times 10^{-3} \times {}^{235}$U	CAIs	4, 55

[a]Environment in which most significant parent–daughter fractionation processes occur.
[b]Half-lives in mega-annum (Ma) (26), except ^{7}Be.
[c]Data from References 110 and 111.
Abbreviations: CAI, calcium-, aluminum-rich inclusion; SLR, short-lived radionuclide.

often dominated by Poisson statistics from the low number of counts. In the isochron diagram used, ^{7}Li/^{6}Li versus ^{9}Be/^{6}Li, both ratios are quite high because of the low natural abundance of ^{6}Li and the need to find high Be/Li phases to detect ^{7}Li excesses. One would expect correlation in the errors of the two quantities, but all published statistical treatments of the data for the ^{7}Be-^{7}Li system regard the two uncertainties as independent. For all these reasons, it cannot be said with confidence that CAIs formed with some live ^{7}Be.

^{10}Be

^{10}Be has a half-life of 1.387 ± 0.012 Ma (26) and decays to ^{10}B. The amount of ^{10}Be inferred in a sample comes from the slope on a ^{10}B/^{11}B versus ^{9}Be/^{11}B internal isochron plot, and the first such convincing isochron in a CAI corresponded to a ^{10}Be/^{9}Be ratio of (9.5 ± 1.9) × 10^{-4} in a CAI (34). Subsequent internal isochrons in CAIs from CV, CH, and CH/CB chondrites (35, 36) show a range of (0.2–10) × 10^{-3}, with the highest ratio of 10^{-2} for a CAI from the Isheyevo CB/CH chondrite (37). There appears to be no correlation between inferred ^{10}Be/^{9}Be ratios in CAIs and ^{26}Al/^{27}Al, which is likely to be a chronometer in CAIs. Inferred ^{10}Be/^{9}Be ratios are from 0.17 × 10^{-3} to 6.1 × 10^{-3} in CAIs from the Sayh al Uhaymir 290 CH and Isheyevo CH/CB chondrites (35). These CAIs contain no detectable excess ^{26}Mg and are inferred to form before ^{26}Al was introduced into the Solar System (although formation after ^{26}Al decay cannot be excluded). These new results are consistent with earlier measurements showing no relationship between ^{26}Al and ^{10}Be, which is to be expected if ^{10}Be is made within the Solar System by spallation from cosmic rays. A measurement of both ^{10}Be/^{9}Be and ^{51}V/^{50}V in six CAIs from two CV3 chondrites found that these quantities covary (38), as expected for solar cosmic-ray irradiation. However, more recently it was found that ^{51}V/^{50}V was well correlated with ^{88}Sr/^{86}Sr, showing that the vanadium and strontium isotopic variations were due to evaporative mass fractionation and unrelated to cosmic-ray irradiation and ^{10}Be production (39). A new study by Dunham et al. (36) has nearly doubled the number of CAIs measured for ^{10}Be-^{10}B systematics through internal isochrons and sought to rectify the overrepresentation of CV chondrite CAIs by analyzing many CAIs from CR, CH/CB, and CO chondrites. These authors also reprocessed literature isochrons to provide a consistent treatment of the entire ^{10}Be-^{10}B data set. They found that most normal CAIs have an inferred ^{10}Be/^{9}Be ratio of ∼7 × 10^{-4}. The data are shown in **Figure 2**, which shows the kernel density estimate (KDE), which peaks at a ^{10}Be/^{9}Be ratio of ∼7 × 10^{-4} for normal CAIs with a tail toward higher values. FUN and PLAC CAIs, which tend to have lower ^{26}Al/^{27}Al and nucleosynthetic isotope anomalies and lower ^{10}Be/^{9}Be values of (4–5) × 10^{-4}, show a broad KDE curve. Also shown are probability distribution function (PDF) curves for all the individual CAIs used to calculate the KDE curves. CAIs with uncertainties of more than 50% of the value were excluded from **Figure 2**. Vermeesch (40) argues that PDF curves, made by summing all the individual PDFs, are not statistically valid and that KDE curves should be used. The normal CAIs have near-canonical values of ^{26}Al/^{27}Al = (4–5) × 10^{-5}, indicating that they formed within ∼200 ka of one another. It was proposed that the ESS ^{10}Be/^{9}Be ratio was ∼7 × 10^{-4} and reflected presolar steady-state production in the interstellar medium and protosolar molecular cloud (36). We adopt the peak value from **Figure 2*a*** for normal, non-FUN CAIs with MSWD values indicating a good isochron fit (36) and uncertainties of less than 50%, (7.3 ± 1.7) × 10^{-4}, for the ESS value, with the uncertainty based on the full width at half maximum of the KDE curve. The KDE curve for FUN CAIs indicates a ^{10}Be/^{9}Be value of (4.5 ± 4.0) × 10^{-4}. There are a few normal CAIs with ^{10}Be/^{9}Be ratios significantly higher than the ESS value. The high values are attributed to local irradiation effects in the Solar System (36). This is consistent with the recent discovery of large excesses in helium and neon in some hibonite-rich CAIs that also formed early in Solar System history (41).

^{26}Al

^{26}Al has a half-life of 0.717 ± 0.024 Ma (26) and decays to ^{26}Mg by positron emission and electron capture. ^{26}Al was one of the first SLRs discovered (42) in a bulk isochron composed of several CAIs. The first ^{26}Mg/^{24}Mg versus ^{27}Al/^{24}Mg internal isochron of a CAI (43) established the ESS ^{26}Al/^{27}Al ratio as (5.1 ± 0.6) × 10^{-5}, a value that has not changed much in the past 45 years. There is no question that there was live ^{26}Al present in the ESS, and the ESS ^{26}Al/^{27}Al ratio in CAIs,

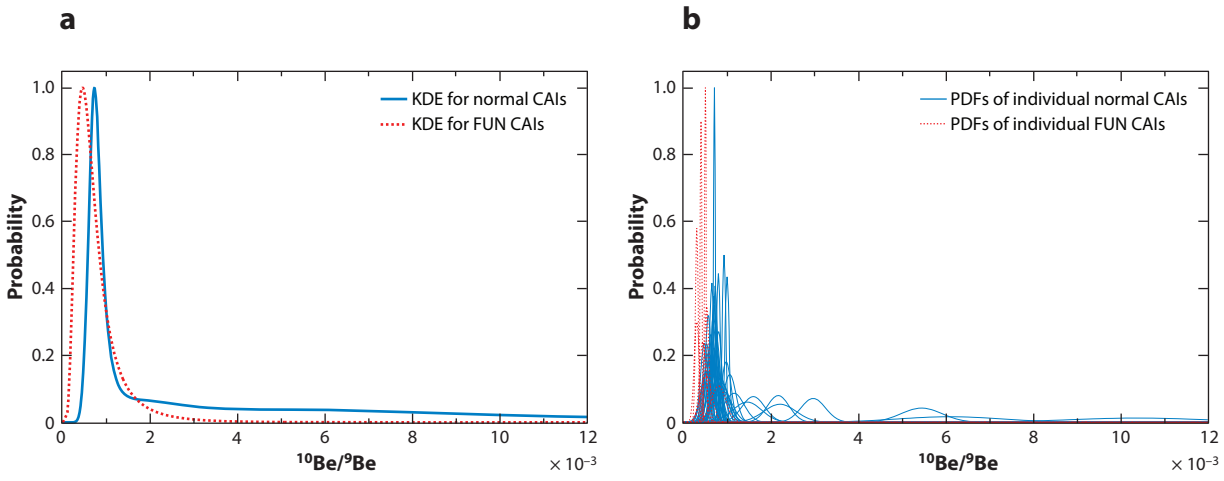

Figure 2

(*a*) KDE (40) diagram of ESS $^{10}Be/^{9}Be$ ratios for normal and FUN CAIs. The two curves are normalized so that they have the same peak height. (*b*) PDFs for individual normal and FUN CAIs. Each PDF has the same area under its curve. Data from Dunham et al. (36), who compiled literature and their own data for CAIs with good isochron fits suggesting no later disturbance, and from one normal CAI from Bekaert et al. (39). CAIs with uncertainties greater than 50% of the value were excluded. The overall distribution of normal CAIs peaks at $^{10}Be/^{9}Be = (7.3 \pm 1.7) \times 10^{-4}$ (±FWHM) with no clear outliers to the low side and a few CAIs with higher $^{10}Be/^{9}Be$. The peak value is considered to be the ESS value inherited from the parental molecular cloud and the high-$^{10}Be/^{9}Be$ tail the result of local Solar System irradiation effects (35). The FUN and PLAC CAIs tend to have lower $^{10}Be/^{9}Be = (4.3 \pm 3.0) \times 10^{-4}$ (±FWHM). Abbreviations: CAI, calcium-, aluminum-rich inclusion; ESS, early Solar System; FUN, fractionation and unidentified nuclear; FWHM, full width at half maximum; KDE, kernel density estimate; PDF, probability distribution function; PLAC, platy crystal.

5.2×10^{-5}, is now well established (44, 45) from bulk isochrons that measure the time of Al/Mg fractionation in the precursors to CAIs. Internal isochrons of individual CAIs show a range of $^{26}Al/^{27}Al$ ratios from near 0 to $\sim 5.2 \times 10^{-5}$ (**Figure 3**).

The data used to construct the isochron composed of several whole CAIs were collected at high precision by MC-ICPMS. Because CAIs have significant mass fractionation effects in magnesium isotopes of a few permil per atomic mass unit, the mass fraction law used can have a significant effect on the slope and intercept of the isochron. The mass fraction law for vacuum evaporation of CAI melts has been measured in the laboratory (13). The law is slightly different from the so-called exponential law that is widely used to correct mass spectrometer data. The widely cited (44) ESS $^{26}Al/^{27}Al$ ratio of $(5.23 \pm 0.13) \times 10^{-5}$ is based on a bulk isochron of several CAIs with mass fractionation corrected with the exponential law. Using the experimentally determined mass fractionation law changes the ESS $^{26}Al/^{27}Al$ ratio to $(5.20 \pm 0.13) \times 10^{-5}$ (44, 45), which we adopt here. The intercept of this isochron is $\delta^{26}Mg^* = -0.040 \pm 029‰$ (44), which agrees with the expected ESS $\delta^{26}Mg^*$ value of −0.038‰ (where terrestrial $\delta^{26}Mg$ is defined as zero). A precise bulk isochron of several whole CAIs and amoeboid olivine aggregates has a slope corresponding to an $^{26}Al/^{27}Al$ ratio of $(5.25 \pm 0.02) \times 10^{-5}$ and an intercept of $\delta^{26}Mg^* = -0.0159 \pm 0014‰$ (46). These data were corrected with an exponential mass fractionation law. An exploration of the effect of the mass fractionation law (13) found that using the experimentally measured mass fraction law significantly affects the data and increases the scatter, because of the range in mass fractionation effects among the individual CAIs. The intercept of the high-precision isochron is significantly different from −0.038‰, and it was proposed that the $^{26}Al/^{27}Al$ ratio in the ESS was heterogeneous and might be lower where chondrules formed (46). Additional data on several CAIs

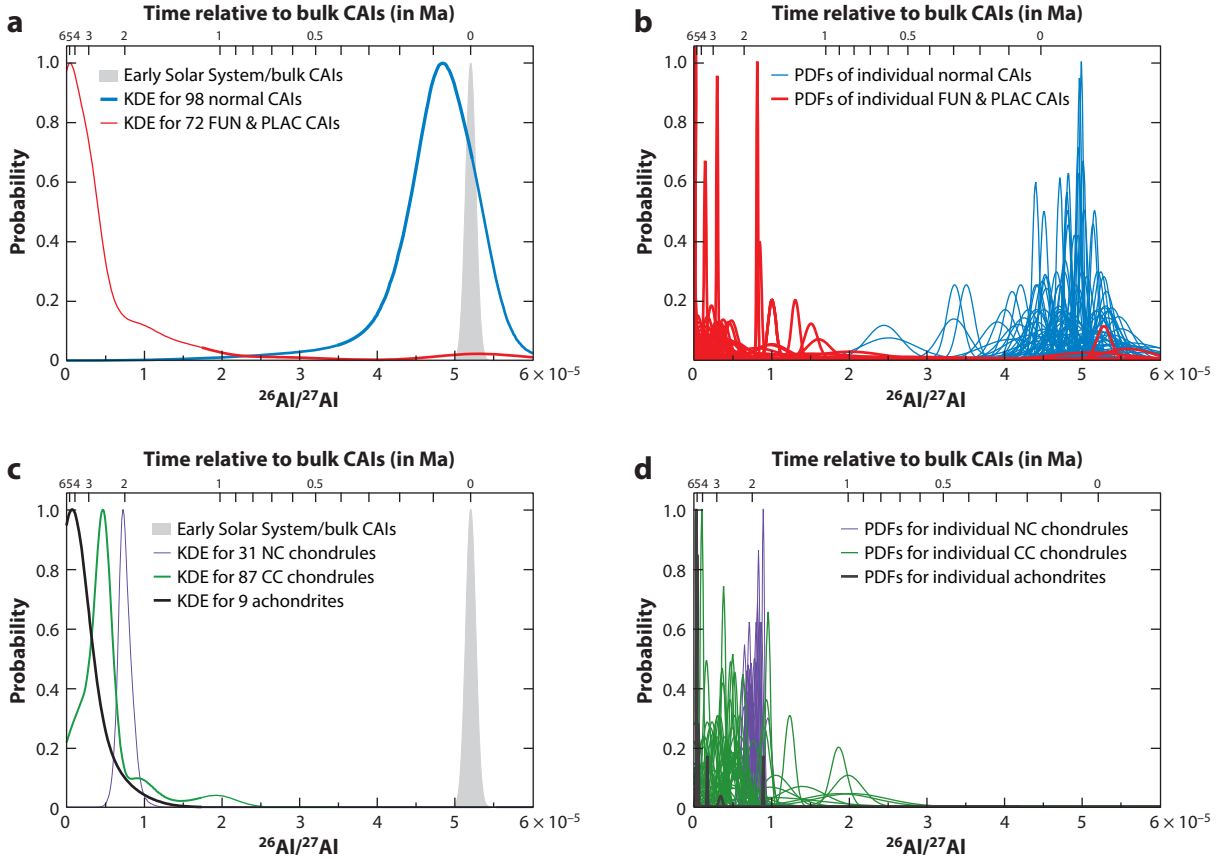

Figure 3

(*a*) KDEs of $^{26}Al/^{27}Al$ in 98 normal and 72 FUN and PLAC CAIs compared with the PDF of bulk CAIs (44, 45), which is taken as the ESS value. The curves are normalized so that they have the same peak height. (*b*) PDFs of $^{26}Al/^{27}Al$ in individual normal and FUN and PLAC CAIs from internal isochrons. Each PDF has the same area under its curve. Internal isochrons were published mostly in the past 10 years (36, 45, 47, 143–146, 150–178). (*c*) KDE of $^{26}Al/^{27}Al$ in 31 chondrules from unmetamorphosed NC meteorites, 87 chondrules from unmetamorphosed CC meteorites, and 9 achondrites, normalized so that they have the same peak height. (*d*) PDFs of $^{26}Al/^{27}Al$ in chondrules in individual achondrites and unmetamorphosed CC and NC chondrites from internal isochrons. Data for CC chondrules (141, 155, 179–189), NC chondrules (142, 190), and achondrites (68, 114, 191–197) are also from the past 10 years or so. The two groups of chondrules have different $^{26}Al/^{27}Al$ distributions, but interpreted as a chronometer, NC and CC chondrules mostly formed ~2.1 and 2.5 Ma, respectively, after CAIs; achondrites crystallized even later. Abbreviations: CAI, calcium-, aluminum-rich inclusion; CC, carbonaceous; ESS, early Solar System; FUN, fractionation and unidentified nuclear; KDE, kernel density estimate; NC, noncarbonaceous; PDF, probability distribution function; PLAC, platy crystal.

from CR chondrites plot along an isochron corresponding to an $^{26}Al/^{27}Al$ ratio of $(5.1 \pm 0.2) \times 10^{-5}$ and a lower intercept of $\delta^{26}Mg^* = -0.095 \pm 026‰$ (47). This finding led to the conclusion that there were at least two CAI reservoirs with different initial magnesium isotopic compositions that produced CAIs at approximately the same time (47).

The major issue today is whether $^{26}Al/^{27}Al$ was homogeneously distributed. To first order, it clearly was not, as the most isotopically anomalous CAIs, FUN inclusions, and PLAC hibonites contained little or no ^{26}Al when they formed, yet they are unlikely to have formed after ^{26}Al decayed. Current thinking is that these odd objects formed in the earliest history of the Solar System and ^{26}Al was introduced afterward. Setting aside the problem of explaining FUN and

PLAC CAIs, there is still the issue of whether ^{26}Al was thoroughly mixed in the solar nebula. There are two camps: one proposing that ^{26}Al was homogeneously distributed and useful as a relative chronometer, implying chondrule formation ~2 Ma after CAIs, and the other proposing that the CAIs formed in an especially ^{26}Al-rich part of the solar nebula and that chondrules and most other objects formed in regions with lower levels of ^{26}Al, implying chondrule formation much closer in time to CAI formation. The finding of two CAI isochrons with similar slope and different initial magnesium isotopic compositions (47) decreases the utility of initial isotopic compositions to obtain chronologic information and weakens the argument for ^{26}Al/^{27}Al heterogeneity. High-precision measurements of several bulk carbonaceous and ordinary chondrites (48) showed that they lie on an isochron with a slope corresponding to $^{26}Al/^{27}Al = (4.67 \pm 0.78) \times 10^{-5}$, within error of the CAI ratio, implying homogeneity of the Solar System ^{26}Al/^{27}Al during formation of CAIs and precursors of chondrules.

Large numbers of internal isochrons of CAIs have been measured by SIMS over the past couple of decades. In **Figure 3**, the KDE curves of CAI isochrons are compared with the bulk value (44, 45). There was a lot of interest in so-called supracanonical isochrons, having slopes corresponding to ^{26}Al/^{27}Al ratios significantly in excess of 5.2×10^{-5} a few years ago (e.g., 49), but as seen in **Figure 3**, there are few if any CAIs with unambiguous supracanonical values. If the CAI-forming region experienced Al/Mg fractionation, which led to the array of compositions that plot on bulk isochrons, one would not expect later melting and crystallization events to lead to internal isochrons with higher slopes. **Figure 3** bears this out. Also shown in **Figure 3** are KDE curves for chondrules from NC and CC groups, as well as achondrites. The recent development of improved primary O^- beams for MC-SIMS has allowed high-quality ^{26}Al-^{26}Mg isochrons to be obtained for chondrules in the most primitive, unmetamorphosed representatives of these two groups. The results indicate chondrule formation at different times for the NC and CC groups, assuming a uniform initial distribution of ^{26}Al/^{27}Al in the Solar System (**Figure 3**). Internal isochrons of achondrites indicate that crystallization of these meteorites occurred after chondrule formation.

^{36}Cl

^{36}Cl is another isotope with a rather short half-life (0.3013 ± 0.0015 Ma) (26) compared to the few-million-years timescale of the ESS. It has a branched decay, with 98.1% forming ^{36}Ar by β^- decay and 1.9% forming ^{36}S by electron capture. It was through excesses in the latter isotope in a mineral with a high Cl/S ratio, sodalite ($NaAlSiO_4 \bullet NaCl$), that the first evidence was found that there was live ^{36}Cl in the ESS (50). This observation was confirmed by Hsu et al. (51) and Jacobsen et al. (52), who showed that ^{36}Cl must have been made after Solar System formation, as the levels were implausibly high for production in stars before Solar System formation. Excess ^{36}S from ^{36}Cl decay has been detected in the minerals sodalite and wadalite [$(Ca,Mg)_6(Al,Fe^{3+})_4((Si,Al)O_4)_3O_4Cl_3$], which are found as secondary alteration phases in refractory inclusions. The inferred ^{36}Cl/^{35}Cl ratios from SIMS measurements of sulfur isotopes range from 0.4×10^{-5} (51) to 1.8×10^{-5} (52). Excess ^{36}Ar from ^{36}Cl decay was detected in another CAI, Allende Pink Angel, corresponding to $^{36}Cl/^{35}Cl = (1.9 \pm 0.5) \times 10^{-8}$ (53). ^{129}I-^{129}Xe dating of the sodalite, the likely host phase of ^{36}Cl, gave a precise age of 4559.4 ± 0.6 Ma, nearly 8 Ma after CAI formation, requiring a local Solar System production mechanism. A detailed calculation of cosmic-ray production of ^{36}Cl under various scenarios led to the conclusion that that implausibly high fluxes of galactic cosmic rays were needed (54). In all the scenarios, nearly all of the ^{36}Cl is made by neutron capture on ^{35}Cl. The most plausible explanation for the apparent isochrons was mixing between chlorine-bearing ice that was exposed to solar cosmic rays for a few Ma and normal isotopic composition sulfur (53); in other words, the isochrons do not provide information on the ^{36}Cl/^{35}Cl ratios at the time

of formation of sodalite or wadalite. Excess ^{36}S uncorrelated with Cl/S (55), as well as excess ^{26}Mg uncorrelated with Al/Mg in a fine-grained CAI with evidence of ^{247}Cm decay (4), was found. Model isochrons based on the bulk Cl/S and Al/Mg ratios led to the conclusion that the object formed with live ^{36}Cl and ^{26}Al early in Solar System history, at the time of canonical $^{26}Al/^{27}Al$, but that near-contemporaneous secondary alteration had redistributed chlorine, sulfur, aluminum, and magnesium with no exchange with an outside reservoir (55). The $^{36}Cl/^{35}Cl$ ratio at the time of secondary alteration was $(2.3 \pm 0.6) \times 10^{-5}$, implying that the ESS $^{36}Cl/^{35}Cl$ ratio was (1.7–3) $\times$ 10^{-5} (55). Thus, much of ^{36}Cl in other CAIs comes from solar cosmic rays, but perhaps there was some early ^{36}Cl of presolar origin. The ESS $^{36}Cl/^{35}Cl$ ratio given in **Table 1** is based on a single unusual CAI and must be considered rather uncertain.

^{41}Ca

Of the confirmed ESS SLRs, ^{41}Ca has the shortest half-life, 0.0994 ± 0.0015 Ma (26). Excess ^{41}K in the Allende CAI Egg-3 was reported by Hutcheon et al. (56), Sahijpal et al. (57), and Ito et al. (58), corresponding to $^{41}Ca/^{40}Ca$ ratios of $(8 \pm 3) \times 10^{-9}$, $(1.17 \pm 0.24) \times 10^{-8}$, and $(4.1 \pm 2.0) \times 10^{-9}$, respectively. Measurement of potassium isotope ratios in samples with high Ca/K ratios by SIMS is difficult, because of the interference of $^{40}Ca^{42}Ca^{2+}$ on the $^{41}K^{+}$ peak. A correction can be made using the $^{40}Ca^{43}Ca^{2+}$ peak at mass 41.5, but the natural $^{43}Ca/^{42}Ca$ ratio is only ~0.2 and the Ca_2^{2+}/Ca^{+} ratio varies among minerals. High-precision ^{26}Al-^{26}Mg dating of CAIs is also important in order to time-correct the inferred $^{41}Ca/^{40}Ca$ ratio to the canonical ESS $^{26}Al/^{27}Al$ ratio of 5.2×10^{-5}. A reexamination of the problem by measuring two Efremovka CAIs previously studied in 1996 (59) with a modern SIMS instrument led to an ESS $^{41}Ca/^{40}Ca$ ratio of $\sim 4.2 \times 10^{-9}$ (60), in agreement with the most recent of the Egg-3 values (58). A high-precision study of ^{26}Al-^{26}Mg systematics of CAIs for which the ^{41}Ca-^{41}K systematics were previously measured found that inferred ESS $^{41}Ca/^{40}Ca$ ratios were somewhat variable, in the range (5.6–13) $\times$ 10^{-9} (61). The last word, for now, comes from a careful study of two CAIs (62), one with a higher $^{41}Ca/^{40}Ca$ ratio (10^{-8}) and one with a lower ratio ($<0.5 \times 10^{-9}$) after correcting each CAI to the ESS $^{26}Al/^{27}Al$ value. It was suggested that there might be three reservoirs in the ESS, with $^{41}Ca/^{40}Ca$ ratios of $<10^{-9}$, $\sim 4 \times 10^{-9}$, and 10^{-8} (62). The value of $\sim 4 \times 10^{-9}$ remains the most commonly observed ratio in CAIs and is adopted as the ESS value.

^{53}Mn

^{53}Mn decays to ^{53}Cr with a somewhat uncertain half-life of 3.7 ± 0.4 Ma (26) and is widely used to measure the relative timing of events in the ESS. Unlike aluminum and hafnium, manganese is not a refractory element, so the ^{53}Mn-^{53}Cr system cannot be anchored to CAIs. Rather, it is usually anchored to a well-studied angrite meteorite, D'Orbigny, which is a rapidly crystallized igneous achondrite. The ESS $^{53}Mn/^{55}Mn$ ratio is inferred by decay-correcting the value measured in D'Orbigny (63) to the time of formation of CAIs. Despite the nonrefractory nature of manganese, the first evidence for the presence of ^{53}Mn in the ESS came from chromium isotopic measurements of CAIs (64). This led to an inferred ESS $^{53}Mn/^{55}Mn$ ratio of $(6.7 \pm 2.2) \times 10^{-5}$, a factor of 10 higher than the generally accepted value inferred by decay-correcting D'Orbigny data using the U-Pb system, 6.8×10^{-6} (65). There are remaining issues with the ESS $^{53}Mn/^{55}Mn$ ratio (66). Comparing D'Orbigny with CAIs, the ^{26}Al-^{26}Mg and ^{182}Hf-^{182}W systems are concordant. Accepting the Pb-Pb age of D'Orbigny, they imply a CAI age of 4568 Ma, 1 Ma older than the average of the four widely accepted uranium-corrected Pb-Pb ages of CAIs, 4567.31 Ma (16), but in agreement with the uranium-corrected Pb-Pb age of a single

CAI, 4567.94 Ma (17). Using the 4567.31 Ma value, the ESS $^{53}Mn/^{55}Mn$ ratio is 6.8×10^{-6}; using 4567.94 Ma, the value is 7.7×10^{-6}. Another angrite anchor, LEW 86010, corrected to a Pb-Pb age of 4568 Ma, was used (67) to obtain an ESS $^{53}Mn/^{55}Mn$ ratio of 9.1×10^{-6}, a value that seems a little too high. Measurements of ^{26}Al-^{26}Mg and ^{53}Mn-^{53}Cr systematics in the unique achondrite NWA 6704 led to the suggestion that, because it is quite old, it might be useful as an anchor point, but a Pb-Pb age is not available (68). A recent study (69) measured uranium isotopes in D'Orbigny to correct the Pb-Pb age. This age was used to time-correct the $^{53}Mn/^{55}Mn$ ratio, taking into account the two Pb-Pb ages for CAIs (16, 17) and resulting in a recommended ESS $^{53}Mn/^{55}Mn$ ratio of $(7 \pm 1) \times 10^{-6}$ (69), which is adopted here.

^{60}Fe

^{60}Fe decays by beta-decay to ^{60}Co, which quickly beta-decays to ^{60}Ni. There have been significant revisions to the half-life of ^{60}Fe, from 0.3 Ma (70) to 1.49 ± 0.27 Ma (71) to the current value of 2.62 ± 0.04 Ma (26, 72). Iron is not a refractory element and its abundance in CAIs is low, so measurements in later-formed objects such as chondrules and achondrites need to be time-corrected to the time of CAI formation. In reading early work on ^{60}Fe, it is important to note which half-life was used in the time-correction. The first evidence for the presence of ^{60}Fe in the ESS came from ^{60}Ni excesses in three bulk samples of the eucrite Chervony Kut, which correlated with Fe/Ni ratios (73). From the ~10 Ma difference between the age of Chervony Kut and CAIs an ESS $^{60}Fe/^{56}Fe$ ratio of $(1.6 \pm 0.5) \times 10^{-6}$ was calculated, but this value was based on the old 1.49 Ma half-life (71). Excess ^{60}Ni was reported for pyroxene from unequilibrated ordinary chondrites (74), from which an ESS $^{60}Fe/^{56}Fe$ ratio of 4×10^{-7} was calculated. However, the SIMS data and some subsequent measurements also by SIMS were affected by inadequate consideration of Poisson statistics for small numbers of counts in the denominators of isotope ratios. Methods of correction for this were developed (75, 76). These methods were applied to published ^{60}Fe-^{60}Ni data (77), with the result that nearly all the SIMS evidence for ESS ^{60}Fe went away. Careful measurement of nickel isotopic compositions in achondrites and chondrites by MC-ICPMS with a clean chemical separation of nickel from iron indicates a low ESS $^{60}Fe/^{56}Fe$ ratio of $(1.01 \pm 0.27) \times 10^{-8}$ (78, 79). An exhaustive study of the ^{60}Fe-^{60}Ni system in chondrules from unequilibrated ordinary chondrites by SIMS (80), using a correction scheme for isotope ratios that takes into account the low count rates (75), found that most chondrules did not contain excess ^{60}Fe, but a few showed excesses, leading to a range of $^{60}Fe/^{56}Fe$ ratios of $(5–30) \times 10^{-8}$ (80). The unique Chicago Instrument for Laser Ionization (CHILI) RIMS instrument (11) was used (81) to study one of the chondrules reported to have excess ^{60}Ni (80). The chondrule did not contain excess ^{60}Ni; the earlier study (80) had not considered error propagation in the correction for mass fractionation effects, leading to underestimation of uncertainties (81). A recent study found small deficits in ^{60}Ni in iron meteorites from groups IID and IVB (82). The ^{182}Hf-^{182}W system was used to measure the time of core formation, and the ESS $^{60}Fe/^{56}Fe$ ratio was found to be $(6.4 \pm 2.2) \times 10^{-7}$ (82). Model calculations of iron and nickel isotopes in type Ia and II supernovae and stellar winds were used to argue that a mixture of nucleosynthetic components could not explain the ^{60}Ni deficits (82); however, nickel isotopic data from presolar grains (83, 84) sample type II supernovae and asymptotic giant branch stars and do not match stellar models that well. Furthermore, the variations in nickel isotopes in the iron meteorites are small and could be of nucleosynthetic origin and unrelated to ^{60}Fe decay. A new NanoSIMS study of troilite in the least metamorphosed chondrites also found low levels of excess ^{60}Ni, further corroborating a low ESS $^{60}Fe/^{56}Fe$ ratio (85). For all these reasons, the ESS $^{60}Fe/^{56}Fe$ ratio of $(1.01 \pm 0.27) \times 10^{-8}$ (79) is recommended and there remains no compelling evidence for higher values.

^{92}Nb

^{92}Nb decays by electron capture to ^{92}Zr with a half-life of 34.7 ± 2.4 Ma (26). It is an interesting isotope, as it is shielded from beta-decay or electron capture by stable ^{92}Mo and ^{92}Zr, so it cannot be made by neutron- or proton-capture nucleosynthesis, leaving photodisintegration as the only viable mechanism for its formation. The first reports of excess ^{92}Zr from ^{92}Nb decay came from zirconium isotopic measurement of a high Nb/Zr rutile (TiO_2) from Toluca IAB iron meteorite (86), leading to an ESS ^{92}Nb/^{93}Nb ratio of $(1.6 \pm 0.3) \times 10^{-5}$. Internal ^{92}Nb-^{92}Zr isochrons on the Estacado H6 ordinary chondrite and the Vaca Muerta mesosiderite led to an ESS ^{92}Nb/^{93}Nb ratio of $\sim 1 \times 10^{-5}$ (87). Further refinement came with measurements of three achondrites with known Pb-Pb ages, leading to an ESS ^{92}Nb/^{93}Nb ratio of $(1.7 \pm 0.6) \times 10^{-5}$ (88). The precision was recently dramatically increased by zirconium isotopic and Nb/Zr measurements on rutile (TiO_2) from several mesosiderites, coupled with Pb-Pb dating of zircon ($ZrSiO_4$) from the same meteorite, leading to the current estimate of the ESS ^{92}Nb/^{93}Nb ratio, $(1.66 \pm 0.10) \times 10^{-5}$ (89). Thus, 25 years of progress have led to great strides in precision, but no significant change in the original value (86).

^{97}Tc and ^{98}Tc

Technetium has two long-lived isotopes that might have been present in the ESS, ^{97}Tc and ^{98}Tc, both of which have half-lives approximately 4.2 Ma (26). As there are no stable isotopes of technetium, the abundances of the technetium SLRs are usually referenced to a molybdenum or ruthenium isotope. Technetium is quite siderophile, allowing an upper limit to the ^{97}Tc/^{92}Mo ratio ($<1 \times 10^{-6}$) to be established from molybdenum isotope measurements in iron meteorites (90). Ruthenium isotopic measurements in iron meteorites were used to establish the ESS ^{98}Tc/^{96}Ru ratio as $<2 \times 10^{-5}$ (91).

^{107}Pd

^{107}Pd decays to ^{107}Ag with a half-life of 6.5 ± 0.3 Ma (26). Palladium and silver are both siderophile, but silver is relatively volatile, so iron meteorites can have high Pd/Ag ratios. Silver has only two stable isotopes, ^{107}Ag and ^{109}Ag, so early measurements by TIMS were limited in precision by mass fractionation effects in mass spectrometers. The first evidence that the ESS contained ^{107}Pd came from excess ^{107}Ag in the Santa Clara IVB iron meteorite measured by TIMS (92). Several subsequent papers from the Caltech Lunatic Asylum used this system to constrain iron meteorite chronology with ^{107}Ag/^{109}Ag versus ^{108}Pd/^{109}Ag internal isochrons (e.g., 93). It was difficult to establish an ESS value because of a lack of high-precision dating of iron meteorite crystallization. The field was revolutionized by the development of MC-ICPMS, which allowed much-higher-precision silver isotopic measurements. A study of the ^{107}Pd-^{107}Ag system in carbonaceous chondrites established an ESS ^{107}Pd/^{108}Pd ratio of $(5.9 \pm 2.2) \times 10^{-5}$ (94). ^{107}Pd-^{107}Ag systematics in the Muonionalusta group IVA iron meteorite were coupled with the measured Pb-Pb age (95) to obtain an ESS ^{107}Pd/^{108}Pd ratio of $(2.8 \pm 0.5) \times 10^{-5}$ (96), a factor of 2 lower than the earlier value (94). However, the Pb-Pb age is based on the assumption that the ^{238}U/^{235}U ratio of the troilite is 137.88, whereas recent measurements of a different sample of Muonionalusta troilite show variable values as low as 137.22 (97). The uranium isotopic ratio of the Muonionalusta troilite sample measured for lead isotopes is not known, so the range of possible ages implies that the ESS ^{107}Pd/^{108}Pd ratio based on Muonionalusta is $(3.50 \pm 0.16) \times 10^{-5}$ to $(6.54 \pm 0.38) \times 10^{-5}$ (98, 99). Silver isotope ratios can also be affected by cosmic-ray exposure in iron meteorites. These effects can be corrected for by measuring platinum isotopes in the same samples (98, 99). The

ESS $^{107}Pd/^{108}Pd$ ratio of $(5.9 \pm 2.2) \times 10^{-5}$ determined from carbonaceous chondrites (94), with its large uncertainty, is still recommended, but this is a problem crying out for a solution.

^{126}Sn

^{126}Sn decays to ^{126}Te with a half-life of 0.230 ± 0.014 Ma (26). It is an r-process isotope, so the short half-life makes it important for understanding other r-process SLRs. The first tellurium isotopic study of carbonaceous chondrites led to an ESS $^{126}Sn/^{124}Sn$ ratio with an upper limit of $<4 \times 10^{-5}$, based on the assumption that no disturbance had occurred since Solar System formation (100). Improvements in analytical techniques for tellurium isotopes and measurements of CAIs led to a ESS $^{126}Sn/^{124}Sn$ ratio with a lower upper limit of $<3 \times 10^{-6}$ (101), adopted here. However, the source of tin and tellurium in CAIs is unclear: It could have entered at the time of CAI formation or it could have been introduced during secondary alteration (101). Both tin and tellurium are relatively volatile elements and not expected to condense into CAI precursors in the solar nebula. If a time-correction of the observed upper limit were necessary, the ESS $^{126}Sn/^{124}Sn$ ratio could be higher.

^{129}I

^{129}I decays to ^{129}Xe with a half-life of 16.14 ± 0.12 Ma (26) and was the first of the SLRs to be discovered (1). Iodine is a highly volatile element, but xenon is even more volatile, so high I/Xe ratios are easily achieved on meteorite parent bodies. The ^{129}I-^{129}Xe system has been extensively used to obtain relative chronology of various meteoritic components. The anchor point for this system is usually Shallowater, an aubrite meteorite (e.g., 102). ^{129}I-^{129}Xe dating is done by irradiating a sample in a nuclear reactor, which turns some stable ^{127}I into ^{128}Xe by neutron capture and beta-decay. The sample is gradually heated and xenon isotopic composition is then measured with a noble gas mass spectrometer. In a well-behaved sample, the thermal release forms an isochron on a $^{129}Xe/^{132}Xe$ versus $^{128}Xe/^{132}Xe$ plot, with the latter ratio serving as a proxy for I/Xe. A sample of Shallowater is irradiated at the same time as the sample and the slopes of the isochrons are compared in order to obtain a date relative to Shallowater. The age of Shallowater is determined by the correlation between I-Xe and Pb-Pb ages of several samples. The age of Shallowater was recently reevaluated with uranium-corrected Pb-Pb ages of these samples and additional I-Xe data to obtain an age of 4562.4 ± 0.2 Ma (103). The $^{129}I/^{127}I$ ratio of Shallowater is $(1.074 \pm 0.014) \times 10^{-4}$ (104). Time-correcting to the two uranium-corrected Pb-Pb ages of CAIs (16, 17) gives ESS $^{129}I/^{127}I$ ratios of 1.33×10^{-4} and 1.37×10^{-4}, so an ESS value $(1.35 \pm 0.02) \times 10^{-4}$ is recommended.

^{135}Cs

^{135}Cs decays to ^{135}Ba with a half-life of 1.33 ± 0.19 Ma (26). The most commonly used half-life is longer, 2.3 Ma, but that is not the main issue with ^{135}Cs. Estimating the ESS $^{135}Cs/^{133}Cs$ ratio is difficult, as cesium is a volatile, fluid-mobile element and barium is refractory and fluid immobile. Furthermore, nucleosynthetic variations in barium isotopes, including ^{135}Ba, in CAIs and bulk chondrites have been demonstrated. The first report of excess ^{135}Ba in acid leachates of CAIs from the Allende CV chondrite was used to infer an ESS $^{135}Cs/^{133}Cs$ ratio of $(4.8 \pm 0.8) \times 10^{-4}$ (105). Further leaching experiments on bulk carbonaceous chondrites and chondrules have led to estimates of the ESS $^{135}Cs/^{133}Cs$ ratio of $(2.7 \pm 1.6) \times 10^{-4}$ (106) and $(6.8 \pm 1.9) \times 10^{-4}$ (107). Excess ^{135}Ba along with much smaller anomalies in other barium isotopes (108) was found in two

CAIs, implying that the ESS $^{135}Cs/^{133}Cs$ ratio might be higher than estimates based on leaching experiments. In a different approach, barium isotopes were measured (109) in angrites and eucrites, two groups of achondrites that have well-constrained ages, an absence of nucleosynthetic barium isotope anomalies, and low Cs/Ba ratios. Because they experienced Rb/Sr fractionation within 1 Ma of CAI formation, Cs/Ba fractionation should have occurred at the same time and they would be expected to have deficits in ^{135}Ba. No such deficits were found and an upper limit of 2.8×10^{-6} was set for the ESS $^{135}Cs/^{133}Cs$ ratio, well below previous estimates (109), and is adopted here. This is a strong argument and the presence of live ^{135}Cs in the ESS must be considered unconfirmed.

^{146}Sm

^{146}Sm decays by alpha-decay to ^{142}Nd with half-life of 103 ± 5 Ma (110, 111). It has proven to be powerful when combined with the long-lived ^{147}Sm-^{143}Nd system, especially for lunar chronology (e.g., 112). The ESS $^{146}Sm/^{144}Sm$ ratio of 0.00828 ± 0.00044 is well-defined by an internal isochron from an igneous CAI (113), which has been superseded by even more precise data from the oldest achondrite known, Erg Chech 002, which gives an ESS $^{146}Sm/^{144}Sm$ ratio of 0.00840 ± 0.00032 (114) and is adopted here. The half-life of ^{146}Sm, however, is in dispute. It does not play a role in the ESS $^{146}Sm/^{144}Sm$ ratio, as this was measured directly in CAIs and in an achondrite so old that it requires no decay-correction, but it is important for chronology of achondrites and lunar rocks. The value of 103 ± 5 Ma was determined by alpha-counting (110, 111). A shorter half-life of 68 ± 7 Ma was determined by accelerator mass spectrometry and alpha-counting (115), but this half-life is inconsistent with ^{146}Sm-^{142}Nd and Pb-Pb age agreement among meteorite and lunar samples (113). Furthermore, the new measurements of the ^{146}Sm-^{142}Nd and ^{26}Al-^{26}Mg systems in Erg Chech 002, coupled with ^{146}Sm-^{142}Nd data on well-dated achondrite and lunar samples, allow a geological determination of the half-life of 102 ± 9 Ma (114), which is in good agreement with the earlier measured half-life of 103 ± 5 Ma. A recent recommendation from the International Union of Pure and Applied Chemistry and the International Union of Geological Sciences (116) proposes using both half-lives, but most isotope geochemists use the longer half-life and perhaps this recommendation can be dropped.

^{182}Hf

With a half-life of 8.90 ± 0.09 Ma (26), ^{182}Hf decays by beta-decay to ^{182}Ta, which quickly decays to ^{182}W. Hafnium and tungsten are efficiently separated from one another during core formation on planetary bodies, as hafnium is lithophile and tungsten is siderophile. Thus, the ^{182}Hf-^{182}W system has been particularly important for studying the chronology of core formation. The ESS $^{182}Hf/^{180}Hf$ ratio, $(1.018 \pm 0.043) \times 10^{-4}$, is well determined from CAIs (117), but nucleosynthetic variations in tungsten isotopes need to be corrected for. Fortunately, the nucleosynthetic tungsten isotopic variations among CAIs are linear and systematic (117). The ^{182}Hf-^{182}W system has been widely applied to chondrites, achondrites, and iron meteorites, as the half-life of ^{182}Hf is long enough to accurately determine relative timescales over a couple of tens of Ma. However, it is important to correct for cosmic-ray effects and small nucleosynthetic tungsten isotopic variations. The current state of the art in studying iron meteorites uses platinum isotopes to correct for cosmic-ray exposure and provides evidence of core formation on planetesimals 1 to 3 Ma after CAI formation (118). Applications of the ^{182}Hf-^{182}W system to planet formation were recently reviewed (119).

^{205}Pb

^{205}Pb decays to ^{205}Tl with a half-life of 17.0 ± 0.9 Ma (26). Both lead and thallium are rather volatile, so this system has seen limited application in ESS chronology. Thallium also has only two stable isotopes, thus ^{205}Tl/^{203}Tl may experience some natural mass fractionation. Furthermore, lead is a common environmental contaminant, leading to uncertainty in Pb/Tl ratios. A ^{205}Tl/^{203}Tl versus ^{204}Pb/^{203}Tl isochron from bulk carbonaceous chondrites led to an ESS ^{205}Pb/^{204}Pb ratio of (1.4 ± 0.4) × 10^{-3} (120). One of those carbonaceous chondrites was found in the desert and its Pb/Tl ratio might have been altered by terrestrial weathering; removing it from consideration led to a somewhat revised recommended ESS ^{205}Pb/^{204}Pb ratio of (1.8 ± 1.2) × 10^{-3} (121).

^{244}Pu

^{244}Pu decays by a series of alpha- and beta-decays to ^{232}Th and eventually to ^{208}Pb, and by spontaneous fission to heavy xenon isotopes, with a half-life of 81.3 ± 0.3 Ma (26). As ^{208}Pb is also made by decay of ^{232}Th made directly by the r-process, the presence of ^{244}Pu in the ESS is inferred from xenon isotopes, making use of the differing fission yield patterns of different natural transuranic isotopes. The ESS ^{244}Pu/^{238}U values from chondrites (0.0068 ± 0.0011; 122) and ancient zircon grains from western Australia (0.0077 ± 0.0006; 123) are in agreement, so the latter value is adopted in **Table 1**.

^{247}Cm

With a half-life of 15.6 ± 0.5 Ma, ^{247}Cm decays by several alpha- and beta-decays to ^{235}U, which in turn eventually decays to ^{207}Pb. The half-life of ^{235}U, 704 ± 1 Ma (26), is long enough that variations in ^{235}U/^{238}U ratios today due to ^{247}Cm decay can be detected. Although small variations in ^{235}U/^{238}U ratios in redox reactions in low-temperature terrestrial environments were known, it came as a shock when it was discovered (3) that there were significant variations in uranium isotope ratios among CAIs. This finding was of profound importance for Pb-Pb dating, which had relied on the assumption that all materials formed with the same ^{235}U/^{238}U ratio and that this ratio changed only through radioactive decay. The uranium isotopic variations led to corrections of up to 5 Ma in Pb-Pb dates of CAIs (3), which had been quoted to precisions of well under 1 Ma. The most accurate Pb-Pb dates of individual CAIs require careful lead and uranium isotopic analysis and there are only five such dates available, four of which give a consistent age of 4567.30 ± 0.16 Ma (15, 16) and one gives 4567.94 ± 0.30 Ma (17). ^{247}Cm decay was considered the most likely explanation for the uranium isotopic variations in CAIs (3), but other causes could not be completely ruled out. The discovery of a 6% excess of ^{235}U in a CAI (4) confirmed ^{247}Cm as the cause, as the effect was too large to allow any other explanation. The ^{247}Cm/^{235}U ratio measured in the Allende CAI Curious Marie was (5.6 ± 0.3) × 10^{-5} (4). It was assumed that aqueous alteration that led to Cm/U fractionation occurred 5 ± 5 Ma after CAI formation, leading to an ESS ^{247}Cm/^{235}U ratio of (7.0 ± 1.6) × 10^{-5} (4). Subsequently, it was found that the event that depleted uranium in Curious Marie also depleted magnesium and that ^{26}Al-^{26}Mg systematics in the CAI show that it formed at the birth of the Solar System (55), so the current recommended ESS ^{247}Cm/^{235}U ratio is the measured value, (5.6 ± 0.3) × 10^{-5} (4).

ORIGINS OF SHORT-LIVED RADIONUCLIDES

The SLRs listed in **Table 1** have a wide variety of origins, some known with more certainty than others. Modeling of nucleosynthesis of stable isotopes and SLRs in stellar environments

has advanced significantly since the main mechanisms of nucleosynthesis were laid out in 1957 (124, 125).

The discovery that ^{26}Al was present in the ESS led to the suggestion that a type II supernova explosion might have triggered the collapse of a molecular cloud to form the Solar System (126); however, the low abundance of ^{60}Fe coupled with a high abundance of ^{26}Al has led to the idea that a Wolf–Rayet star might have provided ^{26}Al in its wind, whereas its subsequent supernova explosion failed to inject any ^{60}Fe. This explanation has been modeled in some detail (127), and production of ^{26}Al, ^{36}Cl, and ^{41}Ca in massive stars and loss through winds have been further explored (128, 129).

The nucleosynthesis of the SLRs has been nicely laid out (130, 131). ^{26}Al can be made in various stellar environments, but it is most efficiently made in the presupernova stages of massive stars. ^{53}Mn is made in these stars also, as is ^{60}Fe. The s-process, which is dominated by low-mass asymptotic giant branch stars, is capable of making several SLRs observed in the ESS, including ^{26}Al, ^{41}Ca, ^{60}Fe, ^{107}Pd, ^{182}Hf, and ^{205}Pb. The r-process, now thought most likely to occur in neutron star mergers, is required to make ^{126}Sn, ^{129}I, ^{244}Pu, and ^{247}Cm and can contribute to ^{107}Pd and ^{182}Hf. The p-process, whose site is unclear, is required to make ^{92}Nb and ^{146}Sm. ^{10}Be is not made in stars and requires formation by spallation of heavier elements. This could take place in the solar nebula or in the interstellar medium prior to Solar System formation. Both ^{41}Ca and ^{36}Cl are made by neutron capture on abundant stable nuclei. Their half-lives are so short that formation in stars requires little time delay between stellar nucleosynthesis and formation of high-temperature (^{41}Ca) and low-temperature (^{36}Cl) minerals in the Solar System.

Several recent papers have modeled SLR formation in stars (127–138). The consensus seems to be that most of the SLRs come from stellar ejecta returned approximately in steady state to the interstellar medium and that the protosolar molecular cloud separated 9–13 Ma before Solar System formation. ^{26}Al requires late injection, perhaps from Wolf–Rayet star winds (127–129), and there are hints from the low ^{26}Al/^{27}Al ratios of FUN and PLAC CAIs that this addition may have occurred after Solar System formation had begun. As an alternative idea, the old supernova trigger model (126) for the cause of Solar System formation has been revised, with the suggestion that an unusual low-mass (11.8 $M_\odot$) core-collapse supernova with explosion energy could have produced many SLRs, including ^{10}Be, through neutrino interactions (138), but such a scenario overproduces ^{53}Mn and ^{60}Fe relative to observations in the Solar System. More recent simulations have resolved this overproduction problem (139, 140).

APPLICATIONS

Relative Chronology

There is great interest in the chronology of events in the early history of the Solar System, including high-temperature condensation and evaporation in the solar nebula, formation of CAIs and chondrules, accretion and differentiation of planetesimals, and planet formation. The only long-lived chronometer with enough precision to study the timing of these events is the U-Pb system, but SLRs offer the opportunity to determine the relative chronology of events. In order to use SLRs for chronology, it needs to be established that the initial Solar System ratio of an SLR to a stable isotope of the same element was uniform. This is usually done by comparison with another SLR or, preferably, the U-Pb system. For such comparisons, it is useful to have anchors, objects that formed in a single event. Commonly used anchors are CAIs and quenched angrites, which are igneous meteorites that crystallized and cooled rapidly. The SLR systems that have been most useful for chronology are ^{26}Al-^{26}Mg, ^{53}Mn-^{53}Cr, ^{107}Pd-^{107}Ag, ^{129}I-^{129}Xe, ^{146}Sm-^{142}Nd, and ^{182}Hf-^{182}W. The parent and daughter isotopes of these systems have various geochemical properties, so

they may be useful for different types of objects. The remaining SLR systems have levels too low to be useful as chronometers.

The ^{26}Al-^{26}Mg system has been widely used for chronology of ESS events. Whether it was uniformly distributed in the Solar System has been questioned (e.g., 46, 47), but the weight of evidence currently suggests that it was. Two of the most important conclusions to come out of the ^{26}Al-^{26}Mg system are that chondrules are of order 2 Ma younger than CAIs (**Figure 3**) and, more recently, that most CC chondrules are younger than NC chondrules (141, 142), which has raised the difficult problem of preserving CAIs in the solar nebula while waiting for chondrules to form and be accreted with CAIs on carbonaceous chondrite parent bodies. The major remaining puzzle is why the CAIs with the largest nucleosynthetic isotope anomalies seem to have formed with low levels of ^{26}Al (143–146). This implies that either they formed after ^{26}Al decayed or they formed early in Solar System history before ^{26}Al was introduced and well mixed. This issue will only be settled by application of another chronometer, either an SLR or the U-Pb system. The latter has proven difficult, as the FUN and PLAC CAIs have low concentrations of uranium. Perhaps the best chance of successfully dating them is with the ^{182}Hf-^{182}W system. This has been done with one FUN CAI (147), showing that it formed early, but more work needs to be done.

The ^{182}Hf-^{182}W system has been particularly important for showing that metallic cores separated from molten planetesimals as soon as 1 Ma after formation of CAIs. The most recent cosmic-ray-corrected ^{182}Hf-^{182}W data show that iron meteorites from the NC group, presumably inside Jupiter's orbit, formed 1–2.2 Ma after CAIs and that those from the CC group, presumably beyond Jupiter's orbit, formed 3.0–3.4 Ma after CAIs (118). ^{53}Mn-^{53}Cr systematics are consistent with this timescale (148). Melting planetesimals so early in Solar System history requires ^{26}Al as a heat source, especially because the ESS ^{60}Fe/^{56}Fe ratio was so low.

The ^{107}Pd-^{107}Ag system is particularly useful for studying iron meteorites, as silver diffusion between metal and troilite (FeS) essentially stops at approximately 500°C. The use of several SLR chronometers has shown the cooling history of the Cape York IIIAB iron meteorite is compatible with the metallographic cooling rate (149).

Melting Planetesimals

Since the discovery that there was ^{26}Al in the ESS, it has been recognized as a potent heat source for melting bodies only a few kilometers in diameter. ^{60}Fe also had the potential of being a heat source, but its ESS abundance is now known to be too low to be an effective heat source. None of the other SLRs in the ESS has high-enough abundances to contribute to heating planetesimals.

OPEN PROBLEMS

The ESS abundances of most SLRs are now well established, but some problems remain. For the most part, the half-lives of the SLRs are measured with adequate precision for use in ESS chronology. One exception is ^{53}Mn, for which the half-life has an uncertainty of more than 10% (26). The other major problem is ^{142}Nd, for which earlier measurements (110, 111) and meteoritic constraints (114) indicate a half-life of 103 Ma, whereas a more recent measurement gives 68 Ma (115). Another measurement of the half-life is desirable.

Some aspects of the SLR record in meteorites remain puzzling. The FUN and PLAC CAIs have large nucleosynthetic isotope anomalies, but they formed with low levels of ^{26}Al. It is plausible that they formed before ^{26}Al was introduced into the Solar System, but there is no independent evidence based on SLRs or long-lived chronometers that they formed before normal CAIs. Further work is also needed to test the consistency among the ^{26}Al-^{26}Mg, ^{53}Mn-^{53}Cr, ^{182}Hf-^{182}W, and U-Pb chronometers.

Finally, further improvements in nucleosynthesis calculations in stars and deeper understanding of stellar winds and mixing with molecular clouds will better constrain the timescales of formation of SLRs in stars and formation of objects in the Solar System that preserve evidence of their decay.

DISCLOSURE STATEMENT

The author is not aware of any affiliations, memberships, funding, or financial holdings that might be perceived as affecting the objectivity of this review.

ACKNOWLEDGMENTS

The author is grateful to an anonymous referee for useful suggestions. This review was supported by the National Aeronautics and Space Administration through grant 80NSSC21K0374.

LITERATURE CITED

1. Reynolds JH. *Phys. Rev. Lett.* 4:8–10 (1960)
2. Urey HC. *PNAS* 41:127–44 (1955)
3. Brennecka GA, et al. *Science* 327:449–51 (2010)
4. Tissot FLH, Dauphas N, Grossman L. *Sci. Adv.* 2:e1501400 (2016)
5. Dauphas N, Chaussidon M. *Annu. Rev. Earth Planet. Sci.* 39:351–86 (2011)
6. Davis AM, McKeegan KD. Short-lived radionuclides and early solar system chronology. In *Treatise on Geochemistry* (ed. HD Holland, KK Turekian), Vol. 1: *Meteorites and Cosmochemical Processes* (ed. AM Davis), pp. 361–95. Oxford, UK: Elsevier. 2nd ed. (2014)
7. Olesik JW. Inductively coupled plasma mass spectrometers. In *Treatise on Geochemistry* (ed. HD Holland, KK Turekian), Vol. 15: *Analytical Geochemistry/Inorganic Instrumental Analysis* (ed. WF McDonough), pp. 309–36. Oxford, UK: Elsevier. 2nd ed. (2014)
8. Carlson RW. Thermal ionization mass spectrometry. In *Treatise on Geochemistry* (ed. HD Holland, KK Turekian), Vol. 15: *Analytical Geochemistry/Inorganic Instrumental Analysis* (ed. WF McDonough), pp. 337–54. Oxford, UK: Elsevier. 2nd ed. (2014)
9. Bizzarro M, et al. *J. Anal. At. Spectrom.* 26:565–77 (2011)
10. Ireland TR. Ion microscopes and microprobes. In *Treatise on Geochemistry* (ed. HD Holland, KK Turekian), Vol. 15: *Analytical Geochemistry/Inorganic Instrumental Analysis* (ed. WF McDonough), pp. 385–409. Oxford, UK: Elsevier. 2nd ed. (2014)
11. Stephan T, et al. *Int. J. Mass Spectrom.* 407:1–15 (2016)
12. Savina M, Trappitsch R. Resonance ionization mass spectrometry (RIMS): Fundamentals and applications including secondary neutral mass spectrometry. In *Photoionization and Photon-Induced Processes in Mass Spectrometry: Fundamentals and Applications*, ed. R Zimmermann, L Hanley, pp. 215–44. Weinheim, Ger.: Wiley-VCH (2020)
13. Davis AM, et al. *Geochim. Cosmochim. Acta* 158:245–61 (2015)
14. Krot AN, et al. Classification of meteorites and their genetic relationships. In *Treatise on Geochemistry* (ed. HD Holland, KK Turekian), Vol. 1: *Meteorites and Cosmochemical Processes* (ed. AM Davis), pp. 1–63. Oxford, UK: Elsevier. 2nd ed. (2014)
15. Amelin Y, et al. *Earth Planet. Sci. Lett.* 300:343–50 (2010)
16. Connelly JN, et al. *Science* 338:651–55 (2012)
17. Bouvier A, Brennecka GA, Wadhwa M. *Absolute chronology of the first solids in the Solar System*. Abstract presented at the Workshop on Formation of the First Solids in the Solar System, Kauai, HI, Nov. 7–9. **https://www.lpi.usra.edu/meetings/solids2011/pdf/9054.pdf** (2011)
18. MacPherson GJ. Calcium–aluminum-rich inclusions in chondritic meteorites. In *Treatise on Geochemistry* (ed. HD Holland, KK Turekian), Vol. 1: *Meteorites and Cosmochemical Processes* (ed. AM Davis), pp. 139–79. Oxford, UK: Elsevier. 2nd ed. (2014)

19. Hu JY, et al. *Sci. Adv.* 7:eabc2962 (2021)
20. Davis AM, Richter FM. Condensation and evaporation of solar system materials. In *Treatise on Geochemistry* (ed. HD Holland, KK Turekian), Vol. 1: *Meteorites and Cosmochemical Processes* (ed. AM Davis), pp. 335–60. Oxford, UK: Elsevier. 2nd ed. (2014)
21. Scott ERD, Krot AN. Chondrites and their components. In *Treatise on Geochemistry* (ed. HD Holland, KK Turekian), Vol. 1: *Meteorites and Cosmochemical Processes* (ed. AM Davis), pp. 65–137. Oxford, UK: Elsevier. 2nd ed. (2014)
22. Warren PH. *Earth Planet. Sci. Lett.* 311:93–100 (2011)
23. Kruijer TS, Kleine T, Borg LE. *Nat. Astron.* 4:32–40 (2020)
24. Burkhardt C, et al. *Sci. Adv.* 7:eabj7601 (2021)
25. Kita NT, et al. *Astron. Soc. Pac. Conf. Ser.* 341:558–87 (2005)
26. Kondev FG, et al. *Chin. Phys. C* 45:030001 (2021)
27. Chaussidon M, Robert F, McKeegan KD. *Geochim. Cosmochim. Acta* 70:224–45 (2006)
28. Podosek FA, et al. *Geochim. Cosmochim. Acta* 55:1083–110 (1991)
29. Leya I. *Geochim. Cosmochim. Acta* 75:1507–18 (2011)
30. Mishra RK, Marhas KK. *Nat. Astron.* 3:498–505 (2019)
31. Richter FM, Davis AM, DePaolo DJ, Watson EB. *Geochim. Cosmochim. Acta* 67:3905–23 (2003)
32. Richter F, Chaussidon M, Mendybaev R, Kite E. *Geochim. Cosmochim. Acta* 182:1–23 (2016)
33. Kunihiro T, Ota T, Nakamura E. *Geochim. Cosmochim. Acta* 252:107–25 (2019)
34. McKeegan KD, Chaussidon M, Robert F. *Science* 289:1334–37 (2000)
35. Fukuda K, et al. *Astrophys. J.* 886:34 (2019)
36. Dunham ET, et al. *Geochim. Cosmochim. Acta* 324:194–220 (2022)
37. Gounelle M, Chaussidon M, Rollion-Bard C. *Astrophys. J.* 763:L33 (2013)
38. Sossi PA, et al. *Nat. Astron.* 1:1–6 (2017)
39. Bekaert DV, et al. *Sci. Adv.* 7:eabg8329 (2021)
40. Vermeesch P. *Chem. Geol.* 312–13:190–94 (2012)
41. Kööp L, et al. *Nat. Astron.* 2:709–13 (2018)
42. Lee T, Papanastassiou DA, Wasserburg GJ. *Geophys. Res. Lett.* 3:109–12 (1976)
43. Lee T, Papanastassiou DA, Wasserburg GJ. *Astrophys. J.* 211:L107–10 (1977)
44. Jacobsen B, et al. *Earth Planet. Sci. Lett.* 272:353–64 (2008)
45. Wasserburg GJ, Wimpenny J, Yin Q-Z. *Meteorit. Planet. Sci.* 47:1980–97 (2012)
46. Larsen KK, et al. *Astrophys. J. Lett.* 735:L37 (2011)
47. Larsen KK, et al. *Earth Planet. Sci. Lett.* 535:116088 (2020)
48. Luu T-H, Hin RC, Coath CD, Elliott T. *Earth Planet. Sci. Lett.* 522:166–75 (2019)
49. Young ED, et al. *Science* 308:223–27 (2005)
50. Lin Y, et al. *PNAS* 102:1306–11 (2005)
51. Hsu W, et al. *Astrophys. J.* 640:525–29 (2006)
52. Jacobsen B, et al. *Astrophys. J.* 731:L28 (2011)
53. Turner G, et al. *Geochim. Cosmochim. Acta* 123:358–67 (2013)
54. Leya I, Masarik J, Lin Y. *Meteorit. Planet. Sci.* 53:1252–66 (2018)
55. Tang H, et al. *Geochim. Cosmochim. Acta* 207:1–18 (2017)
56. Hutcheon ID, Armstrong JT, Wasserburg GJ. *Meteoritics* 19:243–44 (1984)
57. Sahijpal S, Goswami JN, Davis AM. *Geochim. Cosmochim. Acta* 64:1989–2005 (2000)
58. Ito M, Nagasawa H, Yurimoto H. *Meteorit. Planet. Sci.* 41:1871–81 (2006)
59. Srinivasan G, Sahijpal S, Ulyanov AA, Goswami JN. *Geochim. Cosmochim. Acta* 62:1823–35 (1996)
60. Liu M-C, Chaussidon M, Srinivasan G, McKeegan KD. *Astrophys. J.* 761:137 (2012)
61. Srinivasan G, Chaussidon M. *Earth Planet. Sci. Lett.* 374:11–23 (2013)
62. Liu M-C. *Geochim. Cosmochim. Acta* 201:123–35 (2017)
63. Glavin DP, Kubny A, Jagoutz E, Lugmair GW. *Meteorit. Planet. Sci.* 39:693–700 (2004)
64. Birck J-L, Allégre CJ. *Geophys. Res. Lett.* 12:745–48 (1985)
65. Göpel C, et al. *Geochim. Cosmochim. Acta* 156:1–24 (2015)
66. Jilly-Rehak CE, Huss GR, Nagashima K. *Geochim. Cosmochim. Acta* 201:224–44 (2017)

67. Nyquist LE, Kleine T, Shih C-Y, Reese YD. *Geochim. Cosmochim. Acta* 73:5115–36 (2009)
68. Sanborn ME, et al. *Geochim. Cosmochim. Acta* 245:577–96 (2019)
69. Tissot FLH, Dauphas N, Grove TL. *Geochim. Cosmochim. Acta* 213:593–617 (2017)
70. Roy J-C, Kohman TP. *Can. J. Phys.* 35:649–55 (1957)
71. Kutschera W, et al. *Nucl. Instrum. Methods Phys. Res. B* 5:430–35 (1984)
72. Rugel G, et al. *Phys. Rev. Lett.* 103:072502 (2009)
73. Shukolyukov A, Lugmair GW. *Science* 259:1138–42 (1993)
74. Tachibana S, Huss GR. *Astrophys. J.* 588:L41–44 (2003)
75. Ogliore RC, Huss GR, Nagashima K. *Nucl. Instrum. Methods Phys. Res. B* 269:1910–18 (2011)
76. Coath CD, Steele RCJ, Lunnon WF. *J. Anal. At. Spectrom.* 28:52–58 (2013)
77. Telus M, et al. *Meteorit. Planet. Sci.* 47:2013–30 (2012)
78. Tang H, Dauphas N. *Earth Planet. Sci. Lett.* 359–360:248–63 (2012)
79. Tang H, Dauphas N. *Astrophys. J.* 802:22 (2015)
80. Telus M, et al. *Geochim. Cosmochim. Acta* 221:342–57 (2018)
81. Trappitsch R, et al. *Astrophys. J.* 857:L15 (2018)
82. Cook DL, Meyer BS, Schönbächler M. *Astrophys. J.* 917:59 (2021)
83. Trappitsch R, et al. *Geochim. Cosmochim. Acta* 221:87–108 (2018)
84. Kodolányi J, et al. *Geochim. Cosmochim. Acta* 221:127–44 (2018)
85. Kodolányi J, et al. *Astrophys. J.* 929:107 (2022)
86. Harper CL Jr. *Astrophys. J.* 466:437–56 (1996)
87. Schönbächler M, et al. *Science* 295:1705–8 (2002)
88. Iizuka T, et al. *Earth Planet. Sci. Lett.* 439:172–81 (2016)
89. Haba MK, et al. *PNAS* 118:e2017750118 (2021)
90. Burkhardt C, et al. *Earth Planet. Sci. Lett.* 312:390–400 (2011)
91. Becker H, Walker RJ. *Chem. Geol.* 196:43–56 (2003)
92. Kelly WR, Wasserburg GJ. *Geophys. Res. Lett.* 5:1079–82 (1978)
93. Chen JH, Papanastassiou DA, Wasserburg GJ. *Geochim. Cosmochim. Acta* 66:3793–810 (2002)
94. Schönbächler M, et al. *Geochim. Cosmochim. Acta* 72:5330–41 (2008)
95. Blichert-Toft J, et al. *Earth Planet. Sci. Lett.* 296:469–80 (2010)
96. Horan MF, Carlson RW, Blichert-Toft J. *Earth Planet. Sci. Lett.* 351–352:215–22 (2012)
97. Brennecka GA, Amelin Y, Kleine T. *Earth Planet. Sci. Lett.* 490:1–10 (2018)
98. Matthes M, et al. *Geochim. Cosmochim. Acta* 169:45–62 (2015)
99. Matthes M, Fischer-Gödde M, Kruijer T, Kleine T. *Geochim. Cosmochim. Acta* 220:82–95 (2018)
100. Fehr MA, et al. *Geochim. Cosmochim. Acta* 69:5099–112 (2004)
101. Brennecka GA, et al. *Geochim. Cosmochim. Acta* 201:331–44 (2017)
102. Hohenberg CM, Pravdivtseva OV. *Chem. Erde* 68:339–51 (2008)
103 Pravdivtseva O, Meshik A, Hohenberg CM, Krot AN. *Geochim. Cosmochim. Acta* 201:320–30 (2017)
104. Gilmour JD, Pravdivtseva OV, Busfield A, Hohenberg CM. *Meteorit. Planet. Sci.* 41:19–31 (2006)
105. Hidaka H, Ohta Y, Yoneda S, DeLaeter JR. *Earth Planet. Sci. Lett.* 193:459–66 (2001)
106. Hidaka H, Yoneda S. *Geochim. Cosmochim. Acta* 75:3687–97 (2011)
107. Hidaka H, Yoneda S. *Sci. Rep.* 3:1330 (2013)
108. Bermingham KR, et al. *Geochim. Cosmochim. Acta* 133:463–78 (2014)
109. Brennecka GA, Kleine T. *Astrophys. J.* 837:L9 (2017)
110. Friedman AM, et al. *Radiochim. Acta* 5:192–94 (1966)
111. Meissner F, Schmidt-Ott WD, Ziegeler L. *Z. Phys. A* 327:171–74 (1987)
112. Borg LE, et al. *Earth Planet. Sci. Lett.* 523:115706 (2019)
113. Marks NE, et al. *Earth Planet. Sci. Lett.* 405:15–24 (2014)
114. Fang L, et al. *PNAS* 119:e2120933119 (2022)
115. Kinoshita N, et al. *Science* 335:1614–17 (2012)
116. Villa IM, et al. *Geochim. Cosmochim. Acta* 285:70–77 (2020)
117. Kruijer TS, et al. *Earth Planet. Sci. Lett.* 403:317–27 (2014)
118. Spitzer F, Burkhardt C, Nimmo F, Kleine T. *Earth Planet. Sci. Lett.* 576:117211 (2021)

119. Kleine T, Walker RJ. *Annu. Rev. Earth Planet. Sci.* 45:389–417 (2017)
120. Baker RGA, et al. *Earth Planet. Sci. Lett.* 291:39–47 (2010)
121. Palk C, et al. *Meteorit. Planet. Sci.* 53:167–86 (2018)
122. Hudson GB, Kennedy BM, Podosek FA, Hohenberg CM. *Proc. Lunar Planet. Sci. Conf.* 19:547–57 (1989)
123. Turner G, et al. *Earth Planet. Sci. Lett.* 261:491–99 (2007)
124. Burbidge EM, Burbidge GR, Fowler WA, Hoyle F. *Rev. Mod. Phys.* 29:548–654 (1957)
125. Cameron AGW. Chalk River Rep. CRL-41 (1957)
126. Cameron AGW, Truran JW. *Icarus* 30:447–61 (1977)
127. Dwarkadas VV, et al. *Astrophys. J.* 851:147 (2017)
128. Brinkman HE, et al. *Astrophys. J.* 884:38 (2019)
129. Brinkman HE, et al. *Astrophys. J.* 923:47 (2021)
130. Lugaro M, Ott U, Kereszturi Á. *Prog. Part. Nucl. Phys.* 102:1–147 (2018)
131. Vescovi D, et al. *Astrophys. J.* 863:115 (2018)
132. Young ED. *Earth Planet. Sci. Lett.* 392:16–27 (2014)
133. Young ED. *Astrophys. J.* 826:129 (2016)
134. Young ED. *Proc. IAU Symp.* 345:70–77 (2020)
135. Côté B, et al. *Astrophys. J.* 878:156 (2019)
136. Côté B, Yagüe A, Világos B, Lugaro M. *Astrophys. J.* 887:213 (2019)
137. Kaur T, Sahijpal S. *Mon. Not. R. Astron. Soc.* 490:1620–37 (2019)
138. Banerjee P, Qian Y-Z, Heger A, Haxton WC. *Nat. Commun.* 7:13639 (2016)
139. Sieverding A, Müller B, Qian Y-Z. *Astrophys. J.* 904:163 (2020)
140. Qian Y-Z. *EPJ Web Conf.* 260:09001 (2022)
141. Fukuda K, et al. *Geochim. Cosmochim. Acta* 322:194–226 (2022)
142. Siron G, Fukuda K, Kimura M, Kita NT. *Geochim. Cosmochim. Acta* 324:312–45 (2022)
143. Ireland TR. *Geochim. Cosmochim. Acta* 52:2827–39 (1988)
144. Liu M-C, et al. *Geochim. Cosmochim. Acta* 73:5051–79 (2009)
145. Park C, et al. *Geochim. Cosmochim. Acta* 200:6–24 (2017)
146. Kööp L, et al. *Geochim. Cosmochim. Acta* 189:70–95 (2016)
147. Holst JC, et al. *PNAS* 110:8819–23 (2013)
148. Anand A, et al. *Geochem. Perspect. Lett.* 20:6–10 (2021)
149. Matthes M, van Orman JA, Kleine T. *Geochim. Cosmochim. Acta* 285:193–206 (2020)
150. MacPherson GJ, et al. *Geochim. Cosmochim. Acta* 321:343–74 (2022)
151. MacPherson GJ, et al. *Astrophys. J.* 811:L117–21 (2010)
152. Kita NT, et al. *Geochim. Cosmochim. Acta* 86:37–51 (2012)
153. MacPherson GJ, et al. *Earth Planet. Sci. Lett.* 331–332:43–54 (2012)
154. Makide K, et al. *Geochim. Cosmochim. Acta* 110:190–215 (2013)
155. Mishra RK, Chaussidon M. *Earth Planet. Sci. Lett.* 390:318–26 (2014)
156. Kawasaki N, et al. *Geochim. Cosmochim. Acta* 169:99–114 (2015)
157. Kööp L, et al. *Geochim. Cosmochim. Acta* 184:151–72 (2016)
158. MacPherson GJ, et al. *Geochim. Cosmochim. Acta* 201:65–82 (2017)
159. Ushikubo T, Tenner TJ, Hiyagon H, Kita NT. *Geochim. Cosmochim. Acta* 201:103–22 (2017)
160. Kawasaki N, et al. *Geochim. Cosmochim. Acta* 221:318–41 (2018)
161. Kööp L, et al. *Geochim. Cosmochim. Acta* 221:296–317 (2018)
162. MacPherson GJ, Defouilloy C, Kita NT. *Earth Planet. Sci. Lett.* 491:238–43 (2018)
163. Kawasaki N, et al. *Earth Planet. Sci. Lett.* 511:25–35 (2019)
164. Krot AN, et al. *Geochemistry* 79:125529 (2019)
165. Liu M-C, Han J, Brearley AJ, Hertwig AT. *Sci. Adv.* 5:eaaw3350 (2019)
166. Simon SB, Krot AN, Nagashima K. *Meteorit. Planet. Sci.* 54:1362–78 (2019)
167. Han J, et al. *Geochim. Cosmochim. Acta* 269:639–60 (2020)
168. Kawasaki N, et al. *Geochim. Cosmochim. Acta* 279:1–15 (2020)
169. MacPherson GJ, Krot AN, Nagashima K. *Meteorit. Planet. Sci.* 55:2519–38 (2020)
170. Wada S, Kawasaki N, Park C, Yurimoto H. *Geochim. Cosmochim. Acta* 288:161–75 (2020)

171. Fahey AJ, Goswami JN, McKeegan KD, Zinner E. *Geochim. Cosmochim. Acta* 51:329–50 (1987)
172. Ireland TR, Compston W. *Nature* 327:689–92 (1987)
173. Ireland TR. *Geochim. Cosmochim. Acta* 54:3219–37 (1990)
174. Ireland TR, Zinner EK, Fahey AJ, Esat TM. *Geochim. Cosmochim. Acta* 56:2503–20 (1992)
175. Sahijpal S, Goswami JN, Davis AM. *Geochim. Cosmochim. Acta* 64:1989–2005 (2000)
176. Liu M-C, et al. *Geochim. Cosmochim. Acta* 73:5051–79 (2009)
177. Williams CD, et al. *Geochim. Cosmochim. Acta* 201:25–48 (2017)
178. Bodénan J-D, et al. *Geochim. Cosmochim. Acta* 286:214–26 (2020)
179. Ushikubo T, et al. *Geochim. Cosmochim. Acta* 109:280–93 (2013)
180. Nagashima K, Krot AN, Huss GR. *Geochem. J.* 48:561–70 (2014)
181. Sano Y, et al. *Geochem. J.* 48:133–44 (2014)
182. Luu T-H, Young ED, Gounelle M, Chaussidon M. *PNAS* 112:1298–303 (2015)
183. Nagashima K, Krot AN, Komatsu M. *Geochim. Cosmochim. Acta* 201:303–19 (2017)
184. Schrader DL, et al. *Geochim. Cosmochim. Acta* 201:275–302 (2017)
185. Bollard J, et al. *Geochim. Cosmochim. Acta* 260:62–83 (2019)
186. Hertwig AT, et al. *Geochim. Cosmochim. Acta* 253:111–26 (2019)
187. Tenner TJ, et al. *Geochim. Cosmochim. Acta* 260:133–60 (2019)
188. Merle R, et al. *Geochim. Cosmochim. Acta* 277:1–20 (2020)
189. Deng Z, et al. *Geochim. Cosmochim. Acta* 299:163–83 (2021)
190. Siron G, Fukuda K, Kimura M, Kita NT. *Geochim. Cosmochim. Acta* 293:103–26 (2021)
191. Spivak-Birndorf L, Wadhwa M, Janney P. *Geochim. Cosmochim. Acta* 73:5202–11 (2009)
192. Goodrich CA, et al. *Earth Planet. Sci. Lett.* 295:531–40 (2010)
193. Bouvier A, Spivak-Birndorf LJ, Brennecka GA, Wadhwa M. *Geochim. Cosmochim. Acta* 75:5310–23 (2011)
194. Koefoed P, et al. *Geochim. Cosmochim. Acta* 183:31–45 (2016)
195. Hublet G, Debaille V, Wimpenny J, Yin Q-Z. *Geochim. Cosmochim. Acta* 218:73–97 (2017)
196. Schiller M, Connelly JN, Bizzarro M. *Meteorit. Planet. Sci.* 52:1233–43 (2017)
197. Srinivasan P, et al. *Nat. Commun.* 9:3036 (2018)